Air-sea interaction processes over the east-asian marginal seas surrounding the Korean peninsula

D. Bala Subrahamanyam, Radhika Ramachandran, S. Indira Rani, B. Prasad Kumar

Ann. Geophys., 25, 1477–1486, 2007
www.ann-geophys.net/25/1477/2007/

Annales Geophysicae

Air-sea interaction processes over the east-asian marginal seas surrounding the Korean peninsula

D. Bala Subrahamanyam[1], **Radhika Ramachandran**[2], **S. Indira Rani**[1], **and B. Prasad Kumar**[3]

[1]Space Physics Laboratory, Vikram Sarabhai Space Centre, Thiruvananthapuram – 695 022, Kerala, India
[2]DOS – Branch Secretariat, IIIrd Floor, Lok Nayaka Bhavan, New Delhi, 110 003, India
[3]Department of Ocean Engineering and Naval Architecture, Centres for Oceans, Rivers, Atmosphere and Land Sciences, Indian Institute of Technology, Kharagpur, Kharagpur, 721 302, West Bengal, India

Received: 10 November 2006 – Revised: 7 May 2007 – Accepted: 19 June 2007 – Published: 30 July 2007

Abstract. In this article, we describe the seasonal variation of air-sea interface fluxes of heat, momentum and moisture over the East Asian Marginal Seas (EAMS) surrounding the Korean Peninsula. Surface layer meteorological observations for a period of about six years obtained from five oceanic buoys deployed in the Yellow Sea, Korean Strait and East (Japan) Sea form the database for this study. With the available database, monthly mean of sensible heat flux, latent heat flux and momentum flux obtained from the present analysis is compared with the existing climatological data over the EAMS.

Keywords. Oceanography: general (Diurnal, seasonal, arid annual cycles; Marginal and semi-closed seas; Marine meteorology)

1 Introduction

In the field of marine meteorological research and ocean-atmosphere interactions, accurate determination of air-sea interface fluxes at the oceanic surface remain one of the most challenging tasks. In general, four principal measurement techniques, viz: eddy correlation, profile, dissipation and bulk aerodynamic methods are used for determination of surface layer turbulent fluxes of momentum, heat and moisture in the Atmospheric Boundary Layer (ABL) over the ocean as well as land (Garratt, 1992; Stull, 1988; Subrahamanyam, 2003; Subrahamanyam and Radhika, 2002; 2003; Subrahamanyam et al., 2006). With a few notable exceptions, bulk aerodynamic method has been widely used for air-sea interaction studies over the global oceans (Blanc, 1987). This method has a special role because it can be used to estimate fluxes from historical sets of marine weather observations of the "bulk" variable (i.e., wind, humidity, pressure, air and sea surface temperature) and also because it was the most practical way to input the surface layer fluxes in a numerical model. In the recent past, there has been significant progress for attaining higher accuracy in estimation of air-sea exchange parameters through improvements in the bulk aerodynamic parameterization schemes and also through the instrumentation used in the field experiments (WCRP-112, 2000; Subrahamanyam, 2003; Subrahamanyam and Radhika, 2002, 2003). Among the various in situ sources of data for the fluxes and flux related variables, ship-based platform and ocean buoys provide the most reliable information. However, ship-borne observations are available for a limited domain in space as well as in time. On the other hand, ocean buoys provide very useful information in terms of a long term time-series of surface layer meteorological parameters, which can be further used for estimation of air-sea interaction parameters for a local region. A majority of modern ocean buoys provide standard surface layer meteorological observations, spectral wave data and ocean current information.

In this research article, we make use of meteorological observations obtained from five oceanic buoys in the East Asian Marginal Seas (EAMS) adjoining the Korean peninsula to investigate the air-sea interaction processes over this region. Surface layer meteorological observations of Sea Surface Temperature (SST), Air Temperature (AT), Wind Speed (WS), Relative Humidity (RH) and Pressure (PRES) obtained from these five oceanic buoys for a period of about six years (1996–2001) form the database for this study. The RH values are converted to the Specific Humidity (SH) values in the analysis, as the SH provide a direct measurement of the amount of water vapor content present in the air-parcel. This piece of research is mainly aimed to present the seasonal variations of air-sea interface fluxes of heat, momentum and moisture over the EAMS region and compare the estimates with the existing climatological datasets. In the present article, we restrict our research to investigate the behaviour of air-sea interface fluxes only; its impact on the ocean wave

Correspondence to: D. Bala Subrahamanyam
(subrahamanyam@gmail.com)

Published by Copernicus Publications on behalf of the European Geosciences Union.

Table 1. Details of five KMA oceanic buoys.

Sl. No.	Geographical location of the buoy	WMO ID	Sea/Oceanic depth	Measurement height	Data availability period
1.	Dukjukdo (YS1) 37°14′ N, 126°01′ E	22 101	Yellow Sea/ 30-m	3-m	July 1996 to Dec 2001
2.	Chilbaldo (YS2) 34°48′ N, 125°42′ E	22 102	Yellow Sea/ 33-m	3-m	Nov 1996 to Dec 2001
3.	Keomundo (KS1) 34°00′ N, 127°30′ E	22 103	Korean Strait/ 80-m	3-m	March 1998 to Dec 2001
4.	Keojedo (KS2) 34°46′ N, 128°54′ E	22 104	Korean Strait/ 84-m	3-m	May 1998 to Dec 2001
5.	Donghae 37°32′ N, 130°00′ E	22 105	East (Japan) Sea/ 1518-m	6-m	May 2001 to Dec 2001

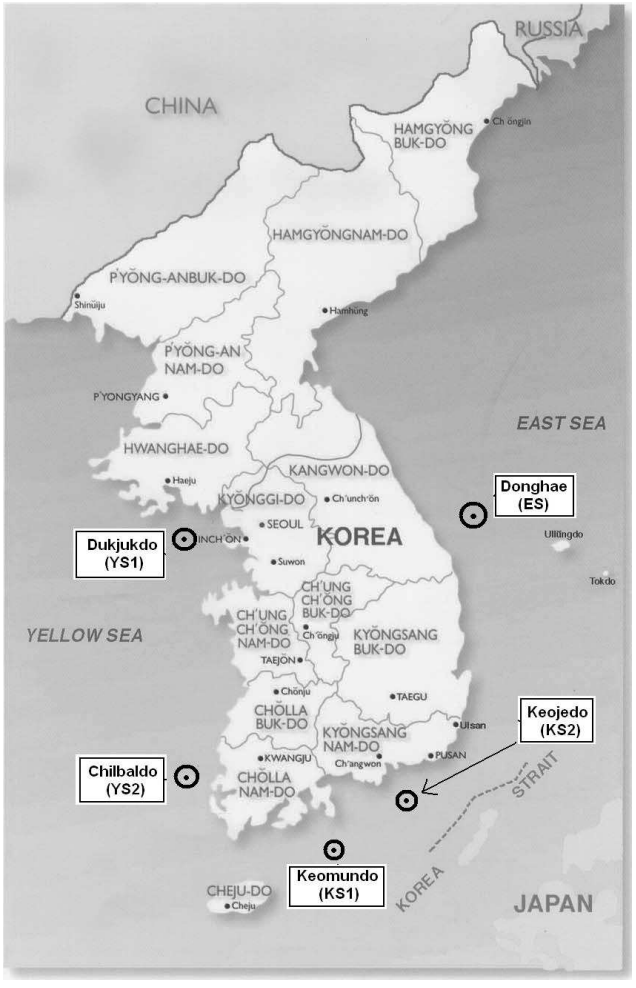

Fig. 1. Location of five KMA Buoys: (1) Dukjukdo – YS1 and (2) Chilbaldo – YS2 (both in Yellow Sea); (3) Keomundo – KS1 and (4) Keojedo – KS2 (both in Korean Strait; (5) Donghae – ES (East Sea).

modelling will be investigated and presented in a separate research article.

2 Data processing and methodology of analysis

The present study on air-sea interaction processes is confined to the EAMS adjoining the Korean Peninsula (Fig. 1). Figure 1 depicts the geographical location of five oceanic buoys operated by Korean Meteorological Administration (KMA). These buoys cover three different oceanic regimes: (a) Yellow Sea; (b) Korean Strait and (c) East Sea (also known as Japan Sea). Some of the important features of these KMA buoys are described in Table 1.

Unlike the measurements made over the land, the oceanic measurements are in general tough to obtain and also the oceanic buoy data need good quality checks, before using them for research purpose. Though, the buoy data does not allow global estimation of the surface fluxes; they are good source of verification of other observing systems. In the modern buoys, in addition to standard surface meteorological data, spectral wave data and current profiles are available for some locations. Due to continuous motion of buoys, the oceanic buoy data can have some errors in the measurements made from this platform. The KMA oceanic buoys provide continuous measurement of surface layer meteorological parameters, such as – SST, AT, WS, RH and Pressure at a regular interval of one hour. In our analysis, 1 January 1996 is considered as Julian day number 1, and accordingly the calendar dates are converted to their corresponding Julian day numbers. In the present analysis, we have projected the raw data to some quality checks to ensure the removal of genuinely bad data points.

In first look, abnormal values of meteorological parameters based on the following criteria are removed from the dataset:

(a) For Sea Surface Temperature:
$-5.0°C \leq SST \leq 40.0°C$

(b) For Air Temperature:
$-25.0°C \leq AT \leq 50.0°C$

(c) For Relative Humidity:
$0\% \leq RH \leq 100.0\%$

(d) For Wind Speeds:
$0\,ms^{-1} \leq WS \leq 50.0\,ms^{-1}$

(e) For Pressure:
$950\,mb \leq PRES \leq 1050\,mb$

After removal of the obvious bad data points based on the criteria mentioned above, individual values beyond three times standard deviation from the mean for each month are considered as the spikes and removed from the raw data (Hirose et al., 1996; Subrahamanyam et al., 2003; Subrahamanyam, 2005). Same procedure is repeated with 2.5 times of the new standard deviation. This kind of quality checks were also suggested by Hirose et al. (1996) for generation of heat budget climatology for the East Sea region, and we believe that it will improve the data quality in the present analysis too, which is further used for preparation of climatological data. After adopting these quality checks, approximately 12% of the raw data points were filtered out.

After incorporation of the above-mentioned quality checks, processed data is projected to the bulk aerodynamic algorithm for estimation of air-sea exchange parameters. In this article, we use the revised bulk aerodynamic algorithm (hereafter referred as SR algorithm) suggested by Subrahamanyam and Radhika (2002, 2003). Detailed methodology adopted in the SR algorithm is described elsewhere (Subrahamanyam, 2003; Subrahamanyam and Radhika, 2002, 2003) and will not be repeated here; however - for the sake of completeness, main equations involved in the SR algorithm are described in Appendix A. It can be seen from the Appendix A, that accurate knowledge of atmospheric stability condition is very crucial for estimation of air-sea interface fluxes of momentum, heat and moisture. Estimates of "z/L" are taken as the indicator of atmospheric stability. Here, "z/L" is referred to as the stability parameter, where "z" is the measurement height and "L" is the Monin-Obukhov length (Garratt, 1992; Stull, 1988). Thus, depending on the magnitudes of stability parameter "z/L", the entire data is categorized into three classes:

Unstable Conditions: $z/L < 0$
Neutral Conditions: $z/L = 0$
Stable Conditions: $z/L > 0$

After adopting such a classification, we obtain the following distribution for unstable, neutral and stable conditions data (Fig. 2). From these in-situ observations it could be seen about 74.03% is unstable condition, while 20.75% is stable condition and remaining 5.22% show a neutral trend (Fig. 2). It has to be noted that – SR algorithm has three set of different equations for estimation of air-sea interaction parameters under different stability stratification (Smith, 1988; Subrahamanyam, 2003; Subrahamanyam and Radhika, 2002, 2003).

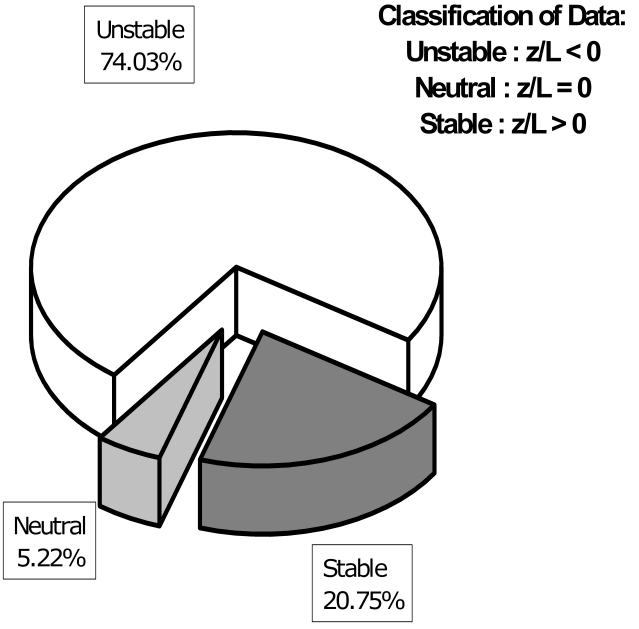

Fig. 2. Pie chart showing the share of unstable, neutral and stable conditions data.

3 Ambient meteorological conditions prevailing over the EAMS

3.1 Yellow Sea

The Yellow Sea is a semi-enclosed basin located between China and Korean peninsula with the Bohai Sea to the northwest and the East China Sea to the south. The Yellow Sea regime is dominated by strong northerly monsoon from late November to March that has an average wind speed in the month of January of approximately $10\,ms^{-1}$ (Yuan and Su, 1984). The month of April happens to be the period of sporadic monsoons, where the wind direction is variable. By the end of May, the southwest monsoon begins. During the summer the wind blows to the north with an average wind speed of about $1.5\,ms^{-1}$ (Mask et al., 1998). Two buoys – located at Dukjukdo and Chilbaldo are taken to be representative of the Yellow Sea region, and are referred to as YS1 and YS2 buoys respectively (Fig. 1). These two buoys provided good database for a period of more than five years from July 1996 to December 2001.

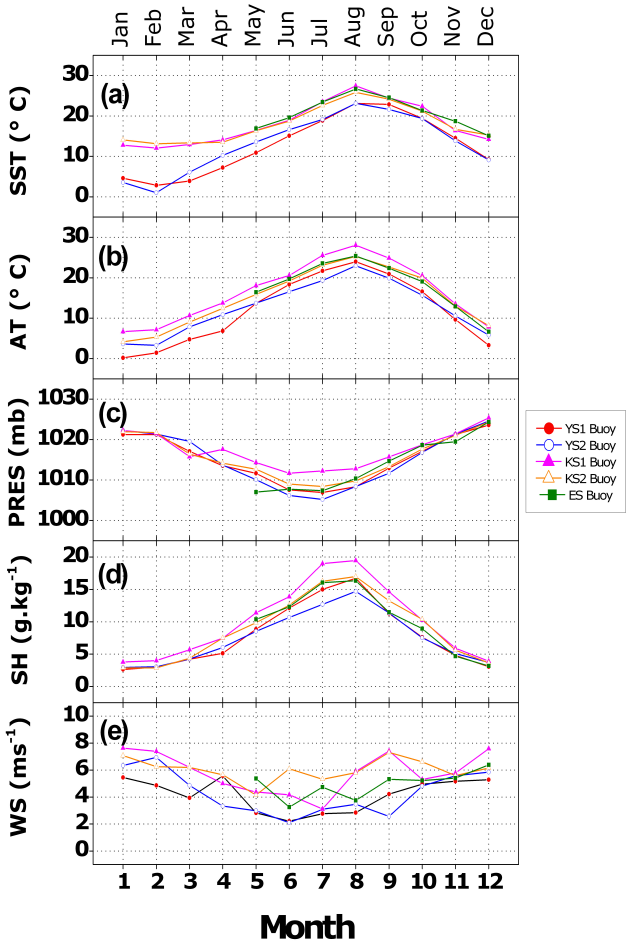

Fig. 3. Monthly mean of **(a)** Sea Surface Temperature (SST), **(b)** Air Temperature (AT), **(c)** Specific Humidity (RH), **(d)** Pressure (PRES) and **(e)** Wind Speed (WS) observed from 5 buoys over EAMS region.

3.2 Korean Strait

The Korean Strait (also referred to as Tsushima Strait) is located in the southwest region of the East Sea and connects the East Sea to the Yellow Sea and the East China Sea. This Strait is well known for prevailing ocean warm currents, as the Tsushima warm current exits the East China Sea through this strait. This warm current dominates the surface layer as it flows northeastward through the Korean Strait and carries warm water into the East Sea (Chu et al., 2001; Minami et al., 1999). This warm current is also the only supplier of heat and salt for the East Sea especially the southern part of East Sea (Lie and Cho, 1994). This is primarily a spring and summer current which is barely discernable in winter. Two buoys located at Keomundo and Keojedo are taken to represent the features of Korean Strait, and are referred to as KS1 and KS2 buoy in this paper (Fig. 1). These buoys were operational from March 1998 and provided reliable database for a period of more than three and half years.

3.3 East Sea (Japan Sea)

The East Sea is a semi-enclosed ocean basin surrounded by four countries of South Korea, North Korea, Russia and Japan. The East Sea is subjected to the seasonal monsoon system. During the winter monsoon, from November through April, a cold northwest wind blows over the East Sea. During the summer monsoon, from mid-May to mid-September, a weaker southeasterly wind blows over the East Sea (Chu et al., 2001). One buoy located at Donghae over the East Sea is referred to as ES buoy in this article. This buoy was installed in the month of May 2001 and about seven months of dataset was available for the analysis.

In Fig. 3, monthly mean of surface layer meteorological parameters – SST, AT, SH Pressure and WS are shown for the five oceanic buoys over the EAMS. In a broad sense, except for the WS (Fig. 3e), all other parameters show sinusoidal pattern for the five buoys (Figs. 3a–d). In case of SST and AT, the peak is seen in the month of August, whereas the minimum values occur during January to February (Figs. 3a and b). On an average, SST varied between 1°C to 27.5°C with a mean of about 16°C, while AT varied from 0°C to 28°C with a mean of about 14.5°C (Figs. 3a and b). In general, SSTs were warmer to ATs by a magnitude of about 1.6°C. Impact of this difference on air-sea interface fluxes is explained in the next section. From Fig. 3a, another interesting observation is – warm SSTs existed over the Korean Strait with relatively cooler SSTs over the Yellow Sea regime. In the summer months, starting from May to November – Korean Strait SSTs were warmer to Yellow Sea SSTs by a magnitude of about 2 to 4°C, whereas this magnitude gets intensified in the rest of the month, attaining a peak of about 11 ° C in the month of February. These warm SSTs over the Korean Strait are due to the influence of Tsushima Warm Ocean current that exits the East China Sea through this Strait. Monthly variations in Pressure for five buoys are shown in Fig. 3c. It can be noticed that – peak in surface pressure (∼1025 mb) occurs during December to February, while minimum values of surface pressure (∼1005 mb) are observed in the month of June–July (Fig. 3c). SH values were varied within a range of about 2 g kg^{-1} to 19 g kg^{-1} (Fig. 3d). Maximum values of SH were observed during the month of July and August, while it remained considerably low (<5 g kg^{-1}) in the month of November to March (Fig. 3d). From the given dataset of about five and half years, we notice that monthly averaged wind speeds varied in the range of 2 to 7.5 ms^{-1} with a mean of about 5 ms^{-1}, where the distribution is found to be chaotic (Fig. 3e). Unlike the seasonal variations observed in SST, AT, PRES and SH, it is noticed that WS do not show any sinusoidal trend over the EAMS.

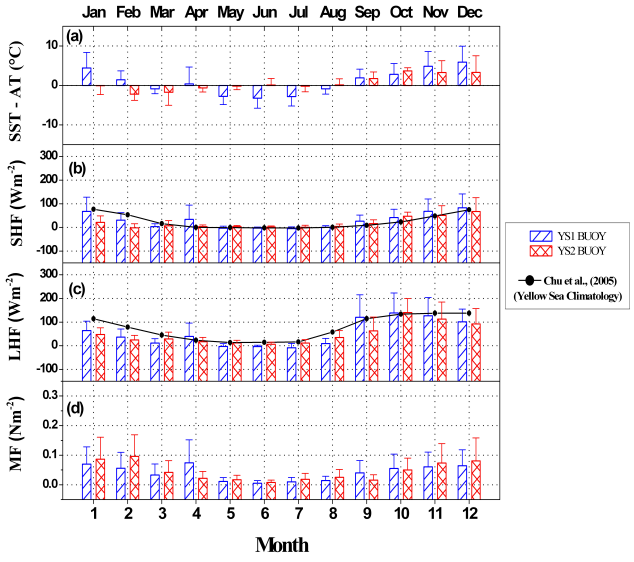

Fig. 4. Monthly mean of **(a)** SST – AT, **(b)** Sensible Heat Flux (SHF), **(c)** Latent Heat Flux (LHF) and **(d)** Momentum Flux (MF) over the Yellow Sea. In panels **(b)** and **(c)**, also shown is monthly variation of SHF and LHF over the Yellow Sea suggested by Chu et al. (2005) – COADS climatology data.

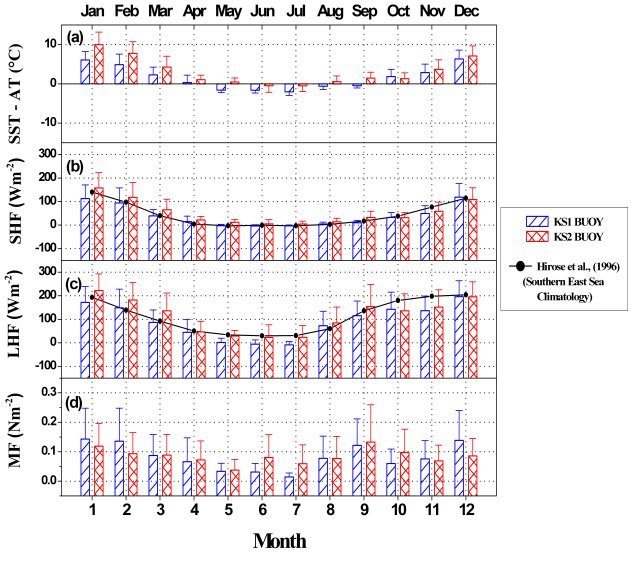

Fig. 5. Same as Fig. 3, but for the Korean Strait. In panel **(b)** and **(c)**, also shown is monthly variation of SHF and LHF over the Southern East Sea suggested by Hirose et al. (1996) – climatology data.

4 Results and discussion

4.1 Seasonal variation of air-sea interface fluxes

In Figs. 4, 5 and 6 – monthly variation of SST – AT (difference of SST with AT, hereafter referred to as DT), SHF, LHF and MF are shown for the Yellow Sea, Korean Strait and East Sea respectively. To compare our estimates of SHF and LHF, we also show the climatology of these parameters for three different oceanic regimes. For the Yellow Sea, we make use of the climatology obtained from $1^\circ \times 1^\circ$ COADS (Comprehensive Ocean-Atmosphere Data Set) for a period of about 44 years spanning from 1945 to 1989 (Chu et al., 2005). For comparison of our estimates of SHF and LHF for the Korean Strait and East Sea, we have taken the climatology data suggested by Hirose et al. (1996). In preparation of heat flux climatology over the East Sea, Hirose et al. (1996) made use of four datasets, viz.: COADS, NODC (National Oceanographic Data Center), JODC (Japan Oceanographic Data Center) and FERHRI (Far Eastern Regional Hydrometeorological Research Institute) for a period of about 31 years from 1960 to 1990. In our comparison, we take the climatology of Northern part of East Sea for the ES buoy, while we compare the climatology of Southern part of East Sea for KS1 and KS2 buoys. Figures 4, 5 and 6 have four panels each, and they depict the monthly variations of – (a) DT, (b) SHF, (c) LHF and (d) MF for the Yellow Sea, Korean Strait and East Sea, respectively.

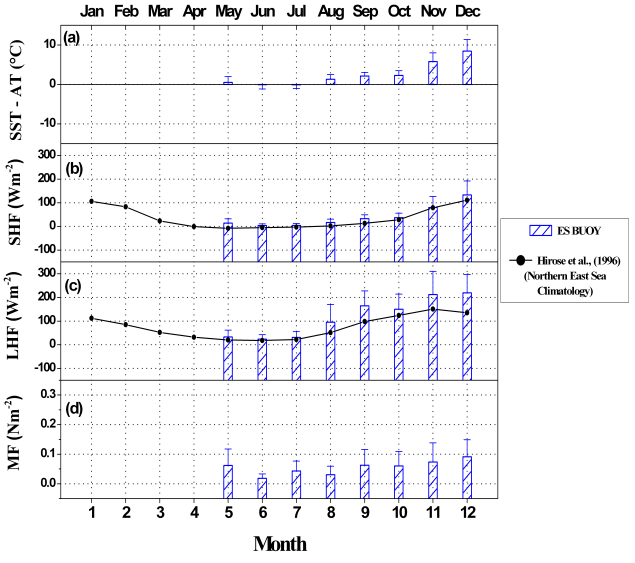

Fig. 6. Same as Fig. 3, but for the East Sea. In panels **(b)** and **(c)**, also shown is monthly variation of SHF and LHF over the Northern East Sea suggested by Hirose et al. (1996) – climatology data.

4.1.1 Yellow Sea

From Fig. 4a, we notice that SSTs are warmer to ATs over the Yellow Sea regime for the month of September to January, while it is reverse for the rest of the months. SHF variations are well in tune with the DT variations. During February to August, very low ($<10\,\mathrm{W\,m^{-2}}$) values of SHF indicate that SST is either equivalent or lesser than AT for that period (Figs. 4a and b). From September onwards, SHF

values start increasing and attains it maximum value of about 65 to 85 $W m^{-2}$ in the month of December, and thereafter it declines with the time (Fig. 4b). These variations are well within the range prescribed by Chu et al. (2005). Monthly variations in LHF also show a sinusoidal trend as that of SHF (Fig. 4c). Minimum values of LHF ($\sim$8.7 $W m^{-2}$ to 12 $W m^{-2}$) are seen in the month of May to July, whereas it peaks ($\sim$140 $W m^{-2}$) in the month of October to November (Fig. 4c). Chu et al. (2005) prescribed a maximum value of LHF of about 137.6 $W m^{-2}$ in the month of November–December, which falls well within the range obtained from the present analysis. Monthly variations in MF for Yellow Sea region are shown in Fig. 4d. No clear trend is evident from the MF data, however – low values of MF occur between May to September, with high values of MF in the rest of the months. These variations seem to be in tune with the WS variations shown in Fig. 4e.

4.1.2 Korean Strait

Similar to Fig. 4, monthly variations of DT, SHF, LHF and MF for the Korean Strait are shown in Fig. 5. Unlike Yellow Sea regime, SSTs are cooler to ATs for the month of May to August, while SSTs are warmer to ATs for the rest of the period (Fig. 5a). Among the two buoys, SST–AT difference for KS2 buoy are always larger than that of the KS1 buoy. And the same trend is also evident in SHF variations, where we notice that – SHF for KS2 buoys are relatively higher than that of the KS1 buoy (Fig. 5b). Analogous to the variations of SHF over the Yellow Sea, Korean Strait also exhibit large values of SHF ($\sim$112 $W m^{-2}$ to 158 $W m^{-2}$) in the month of December to January, and low values of SHF (~ -4 $W m^{-2}$ to 5 $W m^{-2}$) in the month of June–July (Fig. 5b). Monthly variations in LHF also show similar behaviour as that of the SHF. LHF remain low in the range of -8 $W m^{-2}$ to 23 $W m^{-2}$ in the month of June–July, whereas it attains a peak of about 195 to 221 $W m^{-2}$ in the month of December–January (Fig. 5c). In Figs. 5b and c, we also show the monthly variation of SHF and LHF suggested by Hirose et al. (1996) for the Southern East Sea. Monthly variations of SHF and LHF obtained from Hirose et al. (1996) climatology exhibit good match with our estimates of SHF and LHF from the two buoys in the Korean Strait. While comparing these estimates over Korean Strait with that over the Yellow Sea, it is very significant to note that the magnitudes of SHF over Korean Strait are almost two times of that observed over the Yellow Sea region. Such a large difference is due to the Tsushima warm ocean current that flows through the Korean Strait. MF variations for Korean Strait also exhibit irregular behaviour (Fig. 5d), and one reason for its chaotic behaviour is high degree of variability in the wind speeds observed over this region (Fig. 5e).

4.1.3 East Sea

The ES Buoy located in the North-West part of the East Sea provided a database for about seven months from May 2001 to December 2001 only; hence we could not incarcerate the variation over an annual scale. Nevertheless, we show the monthly variations in DT, SHF, LHF and MF for the ES Buoy in Fig. 6. With the available dataset, we notice that SST–AT magnitudes tend to increase from June to December, and attains peak of about 8.5°C in the month of December (Fig. 6a). In line with the variations of SST–AT, SHF also show an increasing trend from June to December (Fig. 6b). In the month of February–March, SHF remains low in the range 2 to 4 $W m^{-2}$, while it peaks to about 133 $W m^{-2}$ in the month of December (Fig. 6b). LHF variations also are found to be similar to that of SHF (Fig. 6c). Peak in LHF occurs in the month of December, where it attains a value of about 219 $W m^{-2}$. In Figs. 6b and c, the monthly climatology of SHF and LHF prescribed by Hirose et al. (1996) for the Northern East Sea are also plotted for skill assessment. MF variations do not exhibit any sinusoidal pattern, as against SHF and LHF variations (Fig. 6d).

Monthly mean of air-sea interface fluxes of momentum, heat and moisture for the three oceanic regions are tabulated in Table 2 for quick reference of the reader.

5 Summary

Availability of surface layer meteorological observations for a period of more than five years spanning from 1996 to 2001 over the adjoining seas of Korean peninsula provided a good opportunity to investigate the underlying physics in the air-sea interaction processes over the EAMS region. Based on five oceanic buoys data deployed at Yellow Sea, Korean Strait and East Sea, monthly variations in air-sea interface fluxes are reported for the study domain. These fluxes are also compared with the available climatology for the EAMS and the estimates fall well within the range prescribed in the climatology (Chu et al., 2005; Hirose, 1996).

Appendix A

Bulk aerodynamic algorithm for estimation of air-sea interaction parameters (SR algorithm; Subrahamanyam and Radhika, 2002, 2003)

The bulk aerodynamic method estimates the turbulent exchanges of downward momentum flux or stress (τ) in $N m^{-2}$, and sensible heat flux (H_S) and latent heat flux (H_L) in $W m^{-2}$. Computation of the surface layer fluxes using this method requires determination of the exchange coefficients for momentum, heat and moisture (C_D, C_H and C_E). The Bulk aerodynamic method has been widely used throughout the marine and air-sea interaction studies for more than three

Table 2. Monthly mean of SHF, LHF and MF for the five buoys. (Here the SHF and LHF units are in $W\,m^{-2}$ and MF units are in $N\,m^{-2}$).

Sl. No.	Buoy name	Flux parameter	Month Jan	Feb	March	April	May	June	July	Aug	Sep	Oct	Nov	Dec	Annual Mean
1	YS1	SHF	67.34	30.66	3.34	33.82	−3.26	−2.87	−4.90	0.66	26.18	41.42	67.85	83.01	28.60
		LHF	63.89	36.61	11.43	39.27	−2.94	−3.39	−8.76	9.53	120.03	138.75	127.06	101.53	52.75
		MF	0.0697	0.0558	0.0329	0.0742	0.0111	0.005	0.0102	0.0141	0.0402	0.0549	0.0608	0.0646	0.0411
2	YS2	SHF	21.26	−1.92	6.61	3.31	3.23	1.75	0.64	4.09	16.05	47.02	50.88	66.82	18.31
		LHF	47.53	24.49	28.83	16.85	12.04	6.34	11.64	34.66	62.96	139.99	112.39	92.12	49.15
		MF	0.0863	0.096	0.042	0.0218	0.0169	0.0079	0.0183	0.0252	0.0157	0.0503	0.0733	0.0808	0.0445
3	KS1	SHF	112.32	94.26	38.76	14.95	−2.45	−4.07	−3.46	4.58	10.07	32.39	49.41	118.66	38.78
		LHF	171.98	148.55	86.51	44.38	1.66	−5.70	−8.71	72.47	115.27	142.23	136.53	195.74	91.74
		MF	0.1428	0.1357	0.0871	0.0662	0.0334	0.0308	0.0141	0.0773	0.1215	0.0601	0.0753	0.1385	0.0819
4	KS2	SHF	157.88	117.80	64.93	21.54	12.07	5.12	4.70	13.88	32.49	31.50	58.93	108.66	52.46
		LHF	221.90	182.04	135.89	46.27	28.53	22.54	23.14	84.61	154.01	135.91	151.65	195.28	115.15
		MF	0.1189	0.0933	0.0887	0.0723	0.0374	0.0802	0.0591	0.0769	0.1327	0.0974	0.069	0.0856	0.0843
5	ES	SHF	–	–	–	–	13.71	3.92	4.16	16.70	32.71	36.99	79.85	132.97	–
		LHF	–	–	–	–	32.89	23.39	30.65	95.30	164.64	149.72	212.30	219.30	–
		MF	–	–	–	–	0.0621	0.0184	0.043	0.0305	0.0627	0.0604	0.0733	0.0914	–

decades now. Considerable effort has gone into the empirical determination of these exchange coefficients; Said and Druilhet (1991) gave an exhaustive survey on the aerodynamic coefficients estimated through different methods over different oceanic regions during various field experiments. In the present analysis, we have estimated the values of exchange coefficients C_D, C_H and C_E through an iterative scheme based on the method suggested by Subrahamanyam and Radhika (2002, 2003). The methodology adopted in this algorithm can be summarized as:

A1 Estimation of friction velocity (u_*) and scaling parameter for temperature (θ_*), and humidity (q_*)

In the atmospheric surface layer, fluxes of momentum, heat and moisture are assumed to be approximately constant, and the mean values of horizontal wind speed, potential temperature, and water vapor density are expected to vary logarithmically with height above the surface for near neutral density stratification. Empirical formulas were derived to account for deviations in the profiles from purely logarithmic in the diabatic case where the density stratification of the layer is different from that for the neutral case (Businger et al., 1971). The integrated forms of these profile relations are given as:

$$u_* = k\,.\,(U_{10} - U_S) \Big/ \left(\ln\left(\frac{z}{z_0}\right) - \Psi_m\right) \tag{A1}$$

$$\theta_* = k\,.\,(\theta_{10} - T_S) \Big/ \left(\ln\left(\frac{z}{z_{0t}}\right) - \Psi_t\right) \tag{A2}$$

$$q_* = k\,.\,(q_{10} - q_S) \Big/ \left(\ln\left(\frac{z}{z_{0q}}\right) - \Psi_q\right) \tag{A3}$$

where U, θ and q represents the mean wind speed (ms^{-1}), potential temperature (K) and specific humidity ($kg\,kg^{-1}$), respectively. The subscripts "$_S$" and "$_{10}$" represent the measurements of the concerned parameter at the sea surface and measurement height, z (=10 m) respectively, T_S is the sea surface temperature (K), k (=0.4) is von Karman constant, u_* is the friction velocity, θ_* and q_* are the scaling parameters for temperature and humidity respectively. In Eqs. (A1–A3), the terms "ψ_m", "ψ_t" and "ψ_q" are the stability functions, whereas z_0, z_{0t} and z_{0q} are the roughness length for winds, temperature and humidity respectively. To initialize the calculations, an estimated value of roughness length, $z_0 \approx 10^{-4}$ m is assumed applicable for the sea surface under moderate wind conditions (Lo, 1993). The values of roughness length for temperature and humidity (z_{0t} and z_{0q}) are determined as described below:

As per the definition of the neutral stability transfer coefficients for heat and moisture (C_{HN} and C_{EN}), Smith (1988) shows that these coefficients are approximately independent of wind speed with values of 1.15×10^{-3} at a reference height of 10-m. These transfer coefficients are given as:

$$C_{HN} = k^2 \Big/ \ln\left(\frac{z}{z_0}\right)\,.\,\ln\left(\frac{z}{z_{0t}}\right) \tag{A4}$$

$$C_{EN} = k^2 \Big/ \ln\left(\frac{z}{z_0}\right)\,.\,\ln\left(\frac{z}{z_{0q}}\right) \tag{A5}$$

Solving the above two equations (Eqs. A4 and A5) with the prescribed value of C_{HN} and C_{EN} (=1.15×10^{-3}) for z_{0t} and z_{0q}, we obtain:

$$z_{0t} = z_{0q} = z \Big/ \exp\left(\frac{k^2}{(1.15\times10^{-3})\,.\,\ln\left(z/z_0\right)}\right) \tag{A6}$$

Thus, with the initial values of z_0 ($\approx10^{-4}$ m), and z_{0t} and z_{0q} estimated from Eq. (A6), we estimate the values of friction

velocity (u_*) and scaling parameters for temperature (θ_*) and humidity (q_*) with the help of the Eqs. (A1–A3). For the first iteration, the stability functions "ψ_m", "ψ_t" and "ψ_q" are assumed to be zero and the wind speed at the sea surface (U_S) is taken as zero (Lo, 1993). The relative humidity at the sea surface is assumed to be 98% (Kraus and Businger, 1994) for the computation of specific humidity (q_S) at the sea surface.

A2 Estimation of integrated stability functions (ψ_m and ψ_h)

As already defined in the above section, ψ_m, ψ_t and ψ_q are the integrated forms of the functions of the lower level stability (z/L), for wind speed, temperature and humidity respectively. The integrated stability functions ψ_m, ψ_t and ψ_q for stable and unstable stratification are defined as (DeCosmo et al., 1996; Dyer, 1974; Smith, 1988):

$$\psi_m = \psi_t = \psi_q = -5.\left(z/L\right) \tag{A7}$$

for stable stratification.

For unstable stratification, the integrated stability functions are defined as (DeCosmo et al., 1996; Paulson, 1970; Smith, 1988):

$$\psi_m = 2\ln\left[(1+x)/2\right] + \ln\left[\left(1+x^2\right)/2\right] - 2\tan^{-1}(x) + \left(\pi/2\right) \tag{A8a}$$

$$\psi_t = \psi_q = 2\ln\left[\left(1+x^2\right)/2\right] \tag{A8b}$$

where "x" is given by:

$$x = \left[1 - 16\left(z/L\right)\right]^{\frac{1}{4}}$$

In the above equations, "L" is the Monin-Obukhov stability length, and it has been derived using (Lo, 1993):

$$L = \left(T_V.u_*^2\right)/\left(k.g.\theta_{V*}\right) \tag{A9}$$

where "g" (=9.8 ms^{-2}) is the acceleration due to gravity. T_V (virtual temperature at the measurement height, in Kelvin) is used in order to include the effects of water vapor content on the density stratification, and θ_{V*} is the scaling parameter for virtual temperature. It can be expressed as a manner similar to Eq. (A2). In the above equations, the ratio (z/L) is called the stability parameter, and its value is positive in stable stratification and negative in unstable stratification. In near-neutral stability conditions, the stability functions vanish.

A3 Estimation of Roughness Length (z_0)

With the estimates of friction velocity obtained from Eq. (A7), we follow the empirical relation for roughness length suggested by Charnock (1955). For the open ocean, the roughness length, due mainly to the shorter surface waves, was postulated to depend on the surface stress based on dimensional considerations by Charnock (1955).

$$z_c = \alpha.u_*^2/g \tag{A10a}$$

where α is an empirically determined constant. Results of numerous field experiments have verified this relationship, with slightly different values of the proportionality constant for open ocean measurements with a fully developed sea state (Wu, 1988). In the present analysis the value of α (=0.011) is assumed after Smith (1988), though Charnock (1955) suggested a value of α=0.012. The roughness length for a smooth surface (e.g., Businger, 1973) depends on the viscosity and the friction velocity (Smith, 1988):

$$z_s = 0.11\,\nu/u_* \tag{A10b}$$

where the dynamic viscosity of air is ν=14×10^{-6} ms^{-1}. The roughness length z_0, or in the other words, the virtual origin of the wind profiles, is obtained by adding z_c and z_s:

$$z_0 = z_c + z_s \tag{A11}$$

Estimates of the roughness length (z_0) are then substituted into Eq. (A6) to obtain the new estimates of roughness length for heat and moisture (z_{0t} and z_{0q}).

The wind speed at sea surface (U_S), commonly known as drift velocity, is generally believed to be zero. However, it has been verified both experimentally and theoretically that the surface drift velocity is approximately equal to u_* (e.g., Hicks, 1972; Lo, 1993; Roll, 1965). Therefore, for the ensuing iterations the estimated value of u_* is substituted in place of drift velocity (U_S) in all the calculations. Now, the estimated values of roughness length (z_0, z_{0t} and z_{0q}) and stability functions (ψ_m, ψ_t and ψ_q) are substituted into Eqs. (A7), (A8) and (A9) to determine the new estimates of u_*, θ_* and q_*.

With the new estimates of u_*, θ_* and q_*, stability functions (ψ_m, ψ_t and ψ_q) and roughness length (z_0, z_{0t} and z_{0q}) are determined again and the iteration is repeated between Eqs. (A1) and (A11) until the u_*, θ_*, q_* and z_0 calculated from two consecutive iterations converge.

A4 Determination of Exchange Coefficients (C_D, C_H and C_E) and the surface layer turbulent fluxes

The estimated values of u_*, θ_* and z_0 are then used for the computation of drag coefficient (C_D), and sensible heat (C_H) and water vapor (C_E) exchange coefficients (Byun, 1990; DeCosmo et al., 1996) using:

$$C_D = u_*^2/(U_{10} - U_S)^2 \tag{A12}$$

$$C_H = u_*.\theta_*/(U_{10} - U_S).(\theta_{10} - T_S) \tag{A13}$$

$$C_E = u_*.q_*/(U_{10} - U_S).(q_{10} - q_S) \tag{A14}$$

Surface fluxes of momentum (τ), heat (H_S) and moisture (H_L) (De Cosmo et al., 1996) are then obtained by substituting C_D, C_H and C_E into:

$$\tau=\rho.C_D.(U_{10}-U_S)^2 \quad \text{(A15)}$$

$$H_S=\rho.C_p.C_H.(U_{10}-U_S).(T_S-T_{10}) \quad \text{(A16)}$$

$$H_L=\rho.L_V.C_E.(U_{10}-U_S).(q_S-q_{10}) \quad \text{(A17)}$$

where "ρ" is the density of moist air, "C_p" is the specific heat of moist air at constant pressure and "L_V" is the latent heat of vaporization.

Acknowledgements. The authors would like to thank I.-C. Pang, Cheju National University, Korea; T.-H. Kim and J.-C. Nam, Marine Meteorological & Earthquake Research Laboratory, Korea Meteorological Administration for making the buoy data available for our analysis. We would also like to extend our gratitude and sincere thanks to R. Sridharan, Director, Space Physics Laboratory for his consistent encouragement to carry out this research work. S. Indira Rani, one of the co-authors, is thankful to Indian Space Research Organization for providing ISRO Research Fellowship for carrying out her Ph.D. thesis work. The revised bulk aerodynamic algorithm (SR algorithm) can be downloaded from authors' webpage (http://www.geocities.com/subbu_dbs/Tools/). We are also thankful to the valuable comments by the anonymous reviewer, which greatly improved the contents of the manuscript.

Topical Editor S. Gulev thanks one anonymous referee for her/his help in evaluating this paper.

References

Blanc, T. V.: Accuracy of Bulk-Method-Determined Flux, Stability, and Sea Surface Roughness, J. Geophys. Res., 92, 3867–3876, 1987.

Businger, J. A.: Turbulent transfer in the atmospheric surface layer, Workshop on Micrometeorology, edited by: Haugen, D. A., American Meteorological Society, Boston, Mass, 67–100, 1973.

Byun, D. W.: On the analytical solutions of flux-profile relationships for the atmospheric surface layer, J. Appl. Meteorol., 29, 652–657, 1990.

Charnock, H.: Wind stress on the water surface, Quart. J. Roy. Meteorol. Soc., 81, 639–640, 1955.

Chu, P., Yuchun, C., and Kuninaka, A.: Seasonal variability of the Yellow Sea/East China Sea Surface Fluxes and Thermohaline Structure, Adv. Atmos. Sci., 22, 1–20, 2005.

Chu, P. C., Lan, J., and Fan, C. W.: Japan/East Sea (JES) seasonal circulation and thermohaline variabilities, Part1, Climatology, J. Phys. Oceanogr., 244–271, 2001.

DeCosmo, J., Kastaros, K. V., Smith, S. D., Anderson, R. J., Oost, W. J., Bumke, K., and Chadwick, H.: Air-Sea Exchange of water vapor and sensible heat: The Humidity Exchange Over the Sea (HEXOS) results, J. Geophys. Res., 101, 12 001–12 016, 1996.

Dyer, A. J.: A review of flux-profile relationships, Bound. Layer Meteorol., 7, 363–372, 1974.

Garratt, J. R.: The Atmospheric Boundary Layer, Cambridge University Press, Cambridge, 316 pp., 1992.

Hicks, B. B.: Propeller anemometers as sensors of atmospheric turbulence, Bound. Layer Meteorol., 3, 214–228, 1972.

Hirose, N., Kim, C. H., and Yoon, J. H.: Head Budget in the Japan Sea, J. Oceanogr., 52, 553–574, 1996.

Kraus, E. B. and Businger, J. A.: Atmosphere-Ocean Interactions, Second Edition, Oxford University Press, New York, 352 pp., 1994.

Lie, H. J. and Cho, C. H.: On the origin of the Tsushima Warm Current, J. Geophys. Res., 99, 25 081–25 091, 1994.

Lo, A. K.-F.: The Direct Calculation of Fluxes and Profiles in the Marine Surface Layer Using Measurements from a Single Atmospheric Level, J. Appl. Meteorol., 32, 1893–1900, 1993.

Mask, C. A., O'Brien, J. J., and Preller, R.: Wind driven effects on the Yellow Sea warm current, J. Geophys. Res., 103, 30 713–30 729, 1998.

Minami, H., Kano, Y., and Ogawa, K.: Long-term variations of potential temperature and dissolved oxygen of the Japan Sea Proper Water, J. Oceanogr., 55, 197–205, 1999.

Paulson, C. A.: The mathematical representation of wind speed and temperature profiles in the unstable atmospheric surface layer, J. Appl. Meteorol., 9, 857–861, 1970.

Roll, H. U.: Physics of the Marine Atmosphere., Academic Press, 426 pp., 1965.

Said, F. and Druilhet, A.: Experimental Study of the Atmospheric Marine Boundary Layer from in-situ aircraft measurements (TOSCANE-T CAMPAIGN): Variability of boundary conditions and Eddy flux parameterization, Bound. Layer Meteorol., 47, 277–293. 1991.

Smith, S. D.: Coefficients for Sea Surface Wind Stress, heat flux and Wind profiles as a function of wind speed and temperature, J. Geophys. Res., 93, 15 467–15 472, 1988.

Stull, R. B.: An Introduction to Boundary Layer Meteorology, Kluwer Academic Publishers, Dordrecht, TheNetherlands, 666 pp, 1988.

Subrahamanyam, D. B.: Detailed Documentation of Wave Model Customization at INCOIS, Updates (January 2005), INCOIS Internal Report, Dept. of Ocean Development, Hyderabad, 88 pp, 2005.

Subrahamanyam, D. B.: Observational and Modelling Studies of the Marine Atmospheric Boundary Layer over the Tropical Indian Ocean during INDOEX, Ph.D. Thesis, Mahatma Gandhi University, Kottayam, Kerala, India, 175 pp (can be downloaded from: http://www.geocities.com/subbu_dbs/CV/Dbs_phd.htm), 2003.

Subrahamanyam, D. B. and Radhika, R.: Wind Speed dependence of Air-Sea Exchange Parameters over the Indian Ocean during INDOEX, IFP-99, Ann. Geophys., 21, 1667–1679, 2003, http://www.ann-geophys.net/21/1667/2003/.

Subrahamanyam, D. B. and Radhika, R.: Air-Sea Interface Fluxes over the Indian Ocean during INDOEX, IFP-99, J. Atmos. Solar Terr. Phys., 64(3), 291–305, 2002.

Subrahamanyam, D. B., Radhika, R., Rani, S. I., Kunhikrishnan, P. K., and Kumar, B. P.: A Comparative Study of Air-Sea Exchange Coefficients and Turbulent Fluxes over Indian Subcontinent and Korean Peninsula, Remote Sensing of Atmosphere and Oceans and Interactions, Proceedings of SPIE, vol. 6404, 640416-1, 12, doi:10.1117/12.694109, 2006.

Subrahamanyam, D. B., Radhika, R., Gupta, K. S., and Mandal, T. K.: Variability of Mixed Layer Heights Over the Indian Ocean

and Central Arabian Sea during INDOEX, IFP-99, Bound. Layer Meteorol., 107, 683–695, 2003.

WCRP – 112: Intercomparison and Validation of Ocean-Atmosphere Energy Flux Fields (Final Report of the Joint WCRP/SCOR Working Group on Air-Sea Fluxes: WMO/TD-No. 1036), 2000.

Wu, J.: On nondimentional correlation between roughness length and wind-friction velocity, J. Oceanogr. Soc. Japan, 44, 254–260, 1988.

Yuan, Y. and Su, J.: Numerical Modelling of the Circulation in the East China Sea, Ocean Hydrodynamics of the Japan and East China Seas, Elsevier Oceanogr. Ser. Elsevier, New York, 39, 167–186, 1984.